

Wear and Corrosion Resistance of Thick Ti-6Al-4V Coating Deposited on Ti-6Al-4V Substrate via High-Pressure Cold Spray

N. W. Khun^{1,2} · A. W. Y. Tan^{1,2} · W. Sun^{1,2} · E. Liu^{1,2}

Submitted: 2 November 2016/in revised form: 1 June 2017
© ASM International 2017

Abstract Ti-6Al-4V (Ti64) coating with a thickness of about 9 mm was deposited on commercial Ti64 substrate via a high-pressure cold spray process. The microstructure, hardness, and wear and corrosion resistance of the Ti64 coating were systematically investigated. The hardness of the Ti64 coating was higher than that of the Ti64 substrate due to the cold-worked microstructure of the coating. The tribological results showed that there was no significant difference in the surface wear rates of the Ti64 coating measured on its different layers while the surface wear resistance of the Ti64 coating was lower than its cross-sectional wear resistance. The corrosion results showed that the Ti64 coating did not effectively prevent its underlying Ti64 substrate from corrosion due to the occurrence of pores in the coating microstructure. It could be concluded that the hardness and wear resistance of the Ti64 coating were comparable to those of the commercial Ti64 substrate.

Keywords cold spray · corrosion · hardness · microstructure · thick Ti-6Al-4V coating · wear

Introduction

The high strength, light weight, and excellent corrosion resistance of titanium (Ti) and its alloys have led to a wide and diversified range of successful applications which demand high levels of reliable performance in aerospace, automotive, chemical plants, power generation, surgery and medicine, oil and gas extraction, and other major industries (Ref 1, 2). Ti-6Al-4V (Ti64) is the most widely used titanium alloy because it features good machinability and excellent mechanical properties (Ref 1, 2). In addition, Ti64 offers the best all-around performance for a variety of weight reduction applications in aerospace, automotive, and marine components (Ref 1, 2).

Ti-based aerospace components are very expensive and require long delivery periods (Ref 1-4). Expensive aerospace components demand repair for wear or corrosion damage during service: Traditionally, thermal spray processes, such as plasma, high velocity oxy-fuel (HVOF), and flame spraying, have been widely used for this purpose (Ref 5-8). However, thermal spray processes could produce metallic coatings with higher porosity and oxidation levels, and higher thermal residual stress than does cold spray process (Ref 9-14). Since Ti64 has poor resistance to high-temperature oxidation, thermal spray processes are not suitable for repair of Ti-based or heat-sensitive aerospace components. Cold spray process can be therefore considered as an alternative process for repair applications because it is a low-temperature process without significant melting of metallic particles to produce metallic coatings with very low porosity and oxidation levels, and lack of thermal stress (Ref 10-15). It is therefore possible to produce thick metallic coatings which are not possible with thermal spray processes. It is clear that the cold spray process would be suitable for repair of Ti-based aerospace

✉ N. W. Khun
khunnaywin@yahoo.com

E. Liu
mejliu@ntu.edu.sg

¹ Rolls-Royce@NTU Corporate Lab, Nanyang Technological University, 50 Nanyang Avenue, Singapore 639798, Singapore

² School of Mechanical and Aerospace Engineering, Nanyang Technological University, 50 Nanyang Avenue, Singapore 639798, Singapore

components. Although 3-mm-thick metallic coatings can be well deposited on metallic substrates via a cold spray process, it becomes challenging to deposit metallic coatings thicker than 3 mm when this is demanded for repair purposes. Thick metallic coatings need to be produced via a cold spray process for successful repair applications.

Ti64 has a drawback encountered with its poor resistance to abrasive wear for rotating or rubbing aerospace components where low wear is crucial (Ref 13, 14, 16, 17). It was reported that cold-sprayed aluminum (Al) alloy coatings had higher wear resistance than their commercial Al alloy substrates (Ref 18). Khun et al. (Ref 12-14, 19) found that the wear resistance of cold-sprayed Ti/Ti64 coatings was higher than their commercial Ti/Ti64 substrates. It is therefore expected that the cold spray process would produce Ti64 coatings with comparable tribological properties to those of commercial Ti64 material. Since the structural and mechanical properties of thick metallic coatings could vary at different layers to affect their tribological properties, the tribological performance of thick Ti64 coatings produced via a cold spray process should be examined at different layers.

Though Ti64 coatings with low porosity levels can be produced by the cold spraying, the presence of intrinsic pores in the cold-sprayed Ti64 coatings affects their corrosion protective performance (Ref 20-22). In the study conducted by Hussian et al. (Ref 21), cold-sprayed Ti coatings did not exhibit an effective corrosion protective performance over their carbon steel substrates. Wang et al. (Ref 22) found that cold-sprayed Ti coatings had higher corrosion current than commercial Ti due to the porous structures of the coatings. It is therefore necessary to investigate the corrosion protective performance of cold-sprayed Ti64 coatings. The private nature of the cold spray technology and its research and development stage greatly limit the available data on the wear and corrosion resistances of cold-sprayed Ti64 coatings (Ref 9, 13, 14). In addition, the wear and corrosion resistances of cold-sprayed Ti64 coatings with thicknesses more than 3 mm have not been reported yet.

In this study, a Ti64 coating with a thickness of about 9 mm was deposited on a commercial Ti64 substrate using a high-pressure cold spray system. The microstructure, hardness, and wear and corrosion resistance of the Ti64 coating were systematically analyzed.

Experimental Details

Sample Preparation

Commercial Ti64 powder (ASTM B348 grade 23, spherical shape, size: 15-45 μm , apparent density: 2.5 g/cm^3) was

purchased from Advanced Powders and Coatings Inc., Canada. Commercial Ti64 substrate with 50 mm \times 50 mm \times 8 mm (Grade 5, Titan Singapore) was used as the substrate on which the Ti64 coating with a thickness of about 8.7-9 mm was deposited using a 5/11 cold spray system (Impact Innovations) with an OUT1 WC nozzle. The type of working gas, gas temperature and pressure, standoff distance, and nozzle speed used were nitrogen (N_2) gas, 1000 $^\circ\text{C}$, 5 MPa, 30 mm, and 300 mm/s, respectively.

To characterize the surface microstructures, hardness, and wear resistances of the Ti64 coating on different layers, all asperities on the surface of the as-deposited Ti64 coating were first completely ground and polished via chemical-mechanical polishing (CMP) process (using a DiaPro solution containing 9- μm diamond particles and an OP-S suspension solution containing 0.04- μm colloidal silica particles (Struers)) to obtain a smooth surface of the so-called first layer (Fig. 1). Then, 2 mm thickness of the same coating was removed via a grinding process with 320-grit papers followed by the CMP process to obtain a smooth surface of the second layer (Fig. 1). Similarly, a smooth surface of the third layer was obtained by removing another 2 mm thickness of the coating (Fig. 1). All the surface characterizations were conducted on the smooth surfaces of the different layers of the Ti64 coating. The cross-sectional microstructure, hardness, and wear resistance were characterized on the cross section of another new Ti64 coating.

Characterization

The surface and wear morphologies of the samples were observed using scanning electron microscopy (SEM) (JEOL-JSM-5600LV).

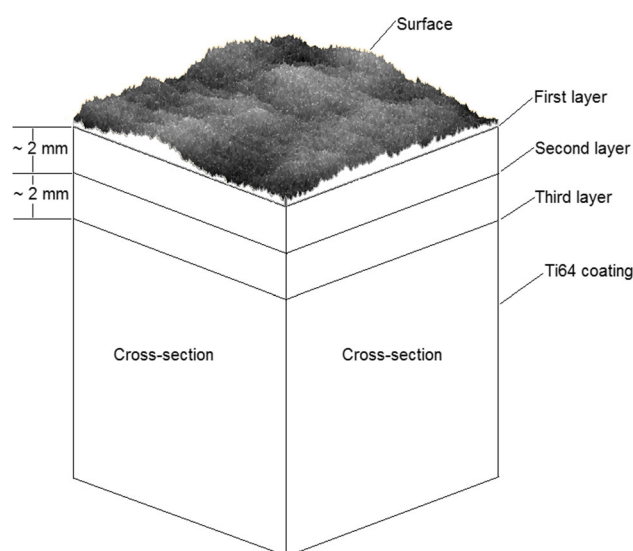


Fig. 1 Schematic diagram of Ti64 coating

The surface and wear topographies of the samples were measured using surface profilometry (SP) (Talyscan 150) with a diamond stylus of 4 μm in diameter. Three measurements per sample were conducted to get an average root-mean-squared surface roughness, R_q .

The microstructure and wear morphology of the samples were evaluated using optical microscopy (OM) (Zeiss Axioskop 2, JVC color video camera). Prior to the microstructural evaluation, the samples were molded with epoxy resin and the molded samples were ground and polished via CMP process (Ref 12-14). At the final stage, the polished samples were etched with Kroll's reagent.

The microstructures of the coating and powder were diagnosed using a Philips MPD 1880 x-ray diffractometer (XRD) with Cu-K α radiation generated at 40 kV and 30 mA.

For the porosity measurement, the OM micrographs of the samples were obtained with $\times 5$ lens before etching and analyzed using ImageJ software. The average surface porosity levels of the Ti64 coating at different layers were obtained by analyzing ten OM micrographs randomly captured on each surface layer. The average cross-sectional porosity level of the Ti64 coating was obtained by analyzing thirty OM micrographs randomly captured on the cross section.

The hardness measurement was conducted using a Vickers micro-indenter (Future-tech FM-300e) under a normal load of 200 g (1.96 N). The surface hardness was averaged from twelve indentation measurements carried out randomly on each surface. A cross-sectional hardness profile was obtained from four indentation measurements performed at every distance from the coating/substrate interface.

A ball-on-disk micro-tribological test (CSM high-temperature tribometer) that conformed to DIN50324 and ASTM G99 was applied to evaluate the tribological properties of the samples. A 100Cr6 steel ball of 6 mm in diameter was fixed on the surface or cross section of the coating rotating in a circular path of 1 mm in radius for 30,000 laps at a sliding speed of 3 cm/s under a normal load of 1 N. Three measurements per surface or cross section were carried out to get average tribological results. The specific wear rates were calculated from the widths and depths of wear tracks measured using SP (Ref 12-14).

Open-circuit potential (OCP) and potentiodynamic polarization measurements were carried out using a Gamry Interface 1000 electrochemical workstation. A flat cell kit with three electrodes was used. All the OCPs and corrosion potentials (E_{corr}) of the samples (working electrode, WE) were measured against a standard Ag/AgCl reference electrode (RE). A platinum mesh was used as the counter electrode (CE). The tested area on the sample was a circle of 1 cm in diameter. A 0.6 M NaCl solution was used for all the measurements. Prior to the electrochemical tests, the as-deposited surfaces of the samples were polished with

1200-grit papers at the final stage to get flat and smooth surfaces followed by ultrasonic cleaning in ethanol and acetone baths, and air drying. The OCP measurement was carried out by exposing the samples to the solution for 24 h. For the polarization measurement, the E_{corr} and corrosion current densities (i_{corr}) of the samples were measured every 3 h at a scan rate of 0.5 mV/s. The corrosion behavior of the samples in the 0.6 M NaCl solution was also investigated using electrochemical impedance spectroscopy (EIS). The EIS measurement was performed using the same electrochemical workstation at their E_{ocp} in a frequency range of 10^5 - 10^{-2} Hz with an AC excitation signal of 10 mV. The corrosion results of the samples were confirmed by two measurements per test.

Results and Discussion

Morphology of Ti64 Particles

Figure 2(a) shows an overview of Ti64 particles used as the initial powder for the fabrication of the Ti64 coating presented in the inset in Fig. 2(b). The spherical particles have a size range from 15 to 45 μm . Figure 2(b) shows the energy-dispersive x-ray (EDX) spectrum of the Ti64 particles on which Ti, Al, and V peaks are found, confirming that the particles used in this study are Ti64 material without significant surface oxidation. The inset in Fig. 2(b) shows the cold-sprayed Ti64 coating with a thickness of about 9 mm on the commercial Ti64 substrate with 50 mm \times 50 mm \times 8 mm. It is confirmed that the thick Ti64 coating has been deposited on the Ti64 substrate without any apparent debonding.

Topography, Morphology, Microstructure, and Porosity of Ti64 Coating

Figure 3(a) shows the surface topography of the as-deposited Ti64 coating on which protruding surface asperities are found. Pores can also be seen on the surface topography. The as-deposited Ti64 coating has R_q of $60.1 \pm 5.2 \mu\text{m}$. Figure 3(b) shows the surface morphology of the as-deposited Ti64 coating on which plastically deformed Ti64 particles can be found. In addition, some pores are consistently found on the surface morphology where sprayed particles are not overlapped onto each other.

Figure 4(a), (b), and (c) shows the similar surface microstructures of the polished Ti64 coating for the first, second, and third layers, respectively, in which individual particles with visible interfaces and a significant number of pores can be clearly seen. In Fig. 4(d), (e), and (f), sprayed particles are interlocked in the surface microstructures of the Ti64 coating observed at the higher magnification.

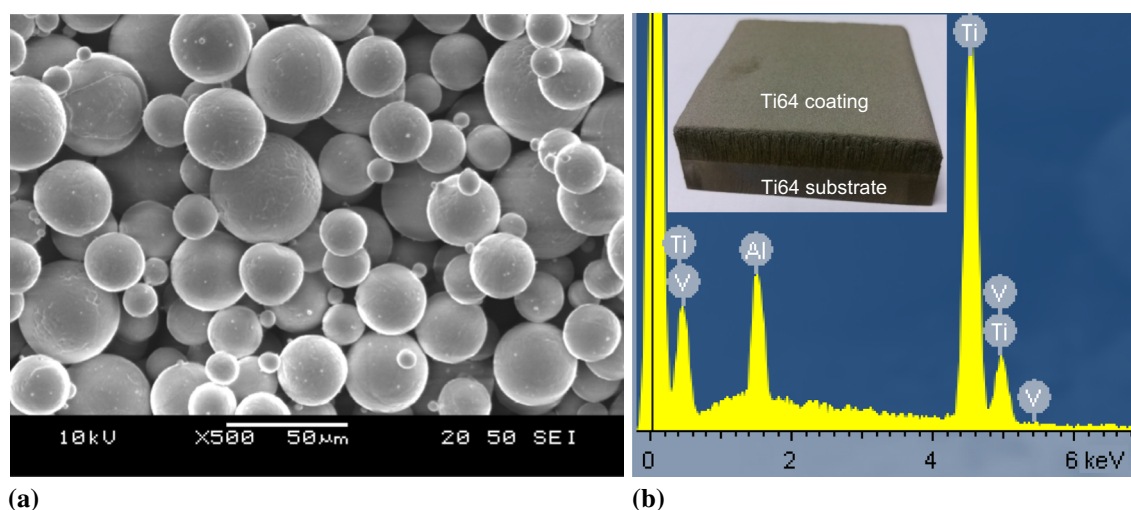
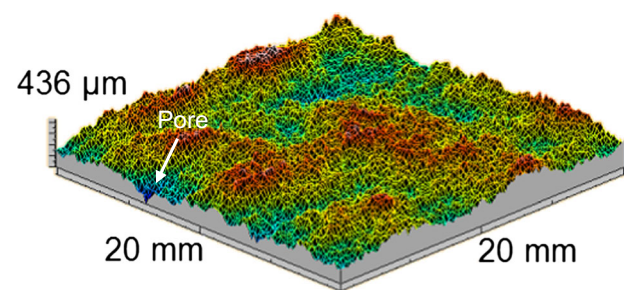
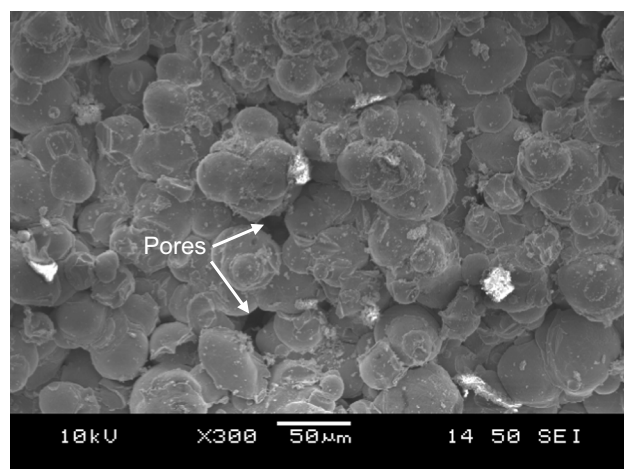


Fig. 2 (a) SEM image showing an overview of Ti64 particles and (b) their EDX spectrum. The inset in (b) shows a photograph of cold-sprayed Ti64 coating on commercial Ti64 substrate



(a)



(b)

Fig. 3 Surface (a) topography and (b) morphology of As-deposited Ti64 coating

Figure 5 shows the cross-sectional microstructures of the Ti64 coating observed at different locations on its cross section. As shown in Fig. 5(a), (b), and (c), individual Ti64 particles with visible interfaces are consistently found in

the microstructures of the coating, while a significant number of pores are found throughout the cross section of the coating. In Fig. 5(d), (e), and (f), irregular-shaped Ti64 particles in the cross-sectional microstructures of the Ti64 coating are indicative of their apparent plastic deformation caused by the high-pressure cold spraying (Ref 8, 9). The severe deformation of the particles results in their interlocking in the cross-sectional microstructures of the Ti64 coating (Fig. 5d, e, and f). As shown in Fig. 5(d), interlocking of sprayed particles gives rise to compact microstructural regions of the Ti64 coating, while bridging of sprayed particles having similar sizes forms pores in the coating microstructure (Fig. 5e).

Figure 5(c) and (f) show the interface between the Ti64 coating and substrate at different magnifications, from which an apparent interfacial gap between the coating and substrate caused by a poor bonding between them is not found (Ref 19). As indicated in Fig. 5(f), a penetration of primary Ti64 particles into the Ti64 substrate is found around primary impact zones (Ref 23). Furthermore, the deformation of secondary particles is influenced by the morphology created by primary particles as shown in Fig. 5(f) (Ref 23).

The average surface porosity levels of the Ti64 coating measured on the first, second, and third layers are 4.6 ± 1.7 , 5.3 ± 1.1 , and $8.2 \pm 0.7\%$, respectively. The average cross-sectional porosity level of the Ti64 coating is $3.5 \pm 0.9\%$. It is clear that the Ti64 coating has lower porosity level in its cross section than in its surface probably due to the more compacted microstructure in the direction of cold spraying.

The typical XRD patterns of the Ti64 powder and Ti64 coating are presented in Fig. 6. The similar XRD patterns between the Ti64 powder and coating show that the cold

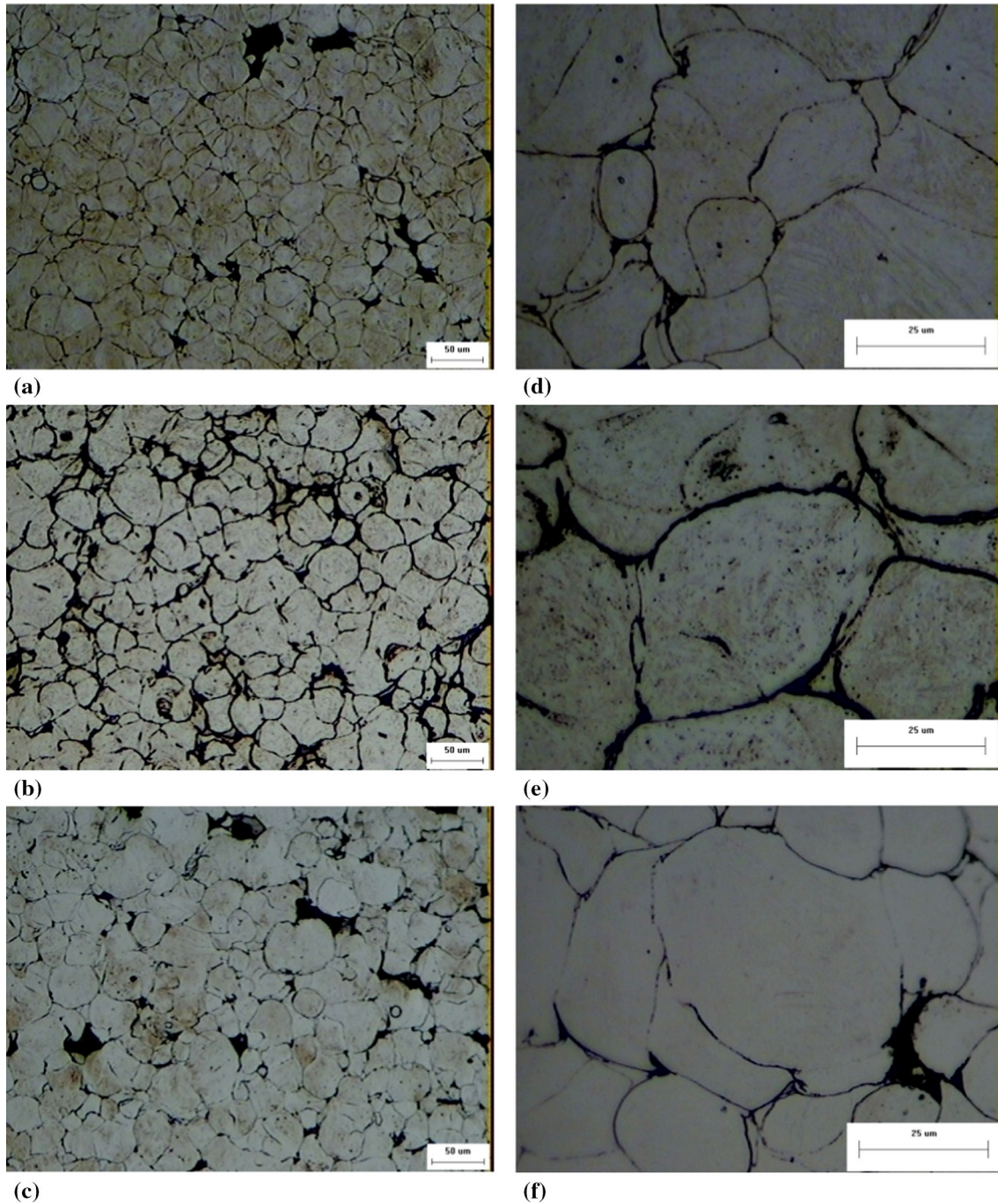


Fig. 4 OM images showing surface microstructures of Ti64 coating, observed at (a, b, and c) low and (d, e, and f) high magnifications after etching, on different layers: (a and d) first, (b and e) second, and (c

and f) third layers. 50 μm and 25 μm scale bars are used for (a, b and c) and (d, e and f), respectively

Hardness of Ti64 Coating

spraying does not cause any apparent phase transformation in the microstructure of the Ti64 coating (Ref 12-14).
The surface hardnesses of the Ti64 coating measured on the first, second, and third layers are 448 ± 26 , 425 ± 14 , and 458 ± 16 $\text{HV}_{0.2}$, respectively. The Ti64 coating does not exhibit

a significant variation in its surface hardnesses on different layers. The surface hardness of the Ti64 substrate is 371 ± 25 $\text{HV}_{0.2}$, implying that the Ti64 coating has higher hardness than the Ti64 substrate due to the cold-worked microstructure of the cold-sprayed coating (Ref 10, 12-14, 19, 24).

Figure 7 presents the hardness of the Ti64 coating measured along its cross section. The Ti64 coating exhibits a uniform hardness over its wide cross section.

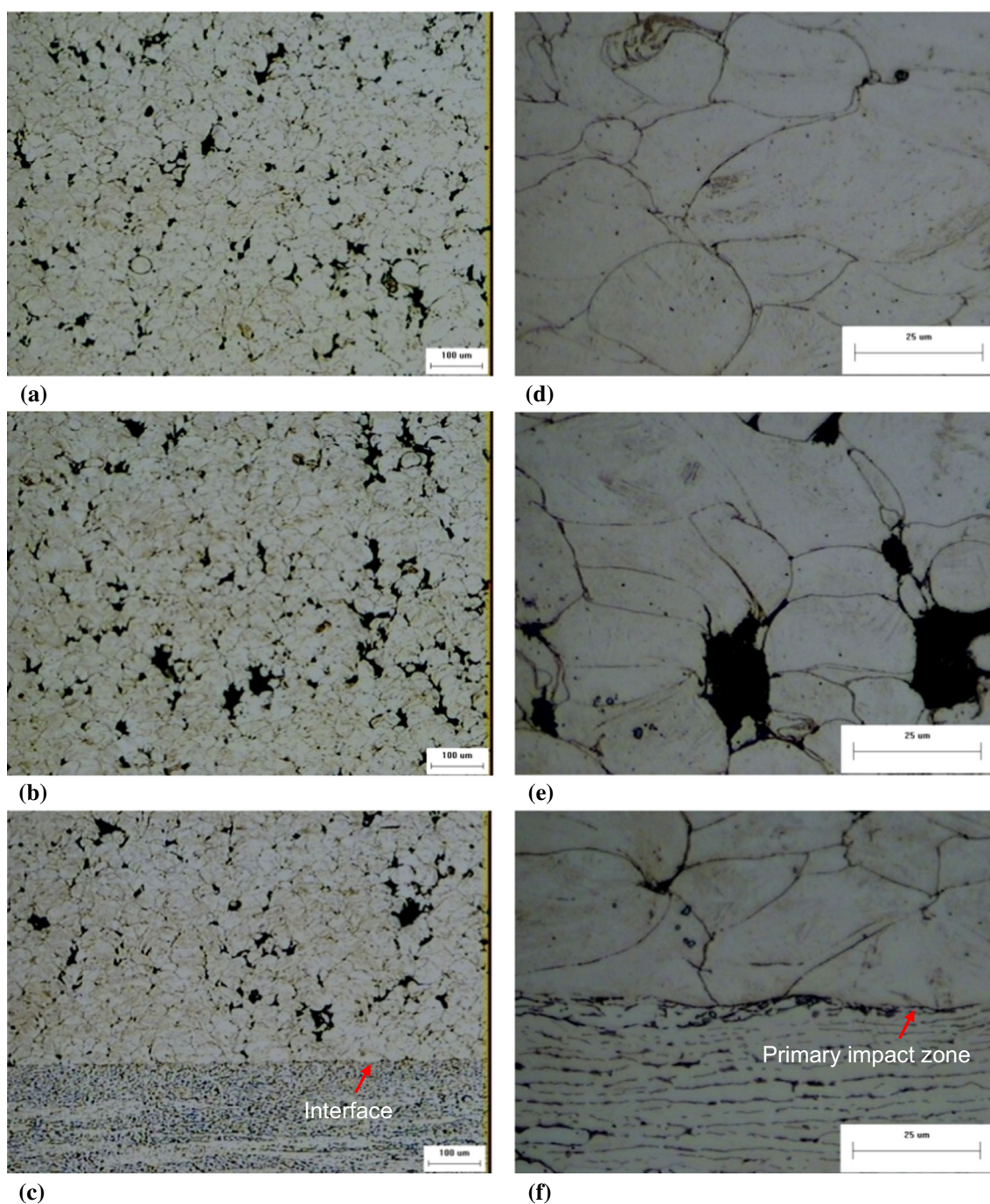


Fig. 5 OM images showing cross-sectional microstructures of Ti64 coating, observed at (a, b, and c) low and (d, e, and f) high magnifications after etching, at different locations: (a and d) top, (b

and e) center, and (c and f) bottom including the coating/substrate interface. 100 μm and 25 μm scale bars are used for (a, b and c) and (d, e and f), respectively

The inset in Fig. 7 shows the surface topography of the polished Ti64 coating with R_q of $0.27 \pm 0.07 \mu\text{m}$ on which pores are found. It was reported in Refs (Ref 12-14) that the R_q of the polished Ti64 substrate was $0.1 \pm 0.01 \mu\text{m}$. It indicates that the existence of pores on the surface of the polished Ti64 coating is responsible for its larger R_q compared to that of the polished Ti64 substrate.

Figure 8(a) and (b) show the indents on the cross-sectional microstructures of the Ti64 substrate and coating made using a normal load of 200 g, respectively. Comparison of Fig. 8(a) and (b) shows that the Ti64 substrate has a larger indent than the Ti64 coating, which is indicative of the lower hardness of the Ti64 substrate than that of the Ti64 coating. In Fig. 8(b), the Ti64 coating has

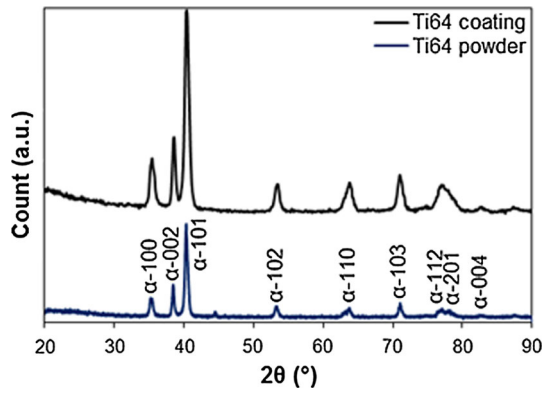


Fig. 6 XRD patterns of Ti64 powder and Ti64 coating

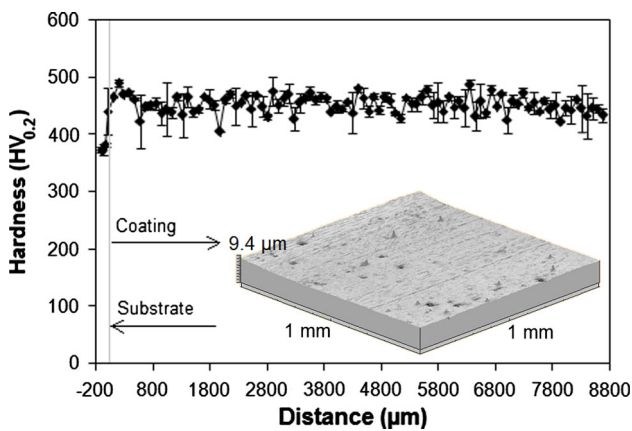


Fig. 7 Cross-sectional hardness of Ti64 coating as a function of the distance from the coating/substrate interface. The gray line represents the coating/substrate interface, and the positive values are “measured distances” for the Ti64 coating from its interface. The inset shows the surface topography of the polished Ti64 coating

the indents with an almost same size for its similar hardness.

Friction and Wear of Ti64 Coating

The friction coefficients and specific wear rates of the Ti64 coating measured on the first, second, and third layers are 0.52 ± 0.01 and $92.9 \pm 16.4 \times 10^{-14} \text{ m}^3/(\text{Nm})$, 0.55 ± 0.03 and $98.6 \pm 15.2 \times 10^{-14} \text{ m}^3/(\text{Nm})$, and 0.5 ± 0.02 and $92 \pm 4.8 \times 10^{-14} \text{ m}^3/(\text{Nm})$, respectively. It is clear that the friction coefficients and specific wear rates of the Ti64 coating measured on its different layers are not very much different from each other as a result of the similar microstructures of all the layers. The friction coefficient and specific wear rate of the commercial Ti64 substrate tested against the steel ball under the same conditions are 0.55 ± 0.01 and $93.9 \times 10^{-14} \text{ m}^3/(\text{Nm})$, respectively. The similar friction coefficients and specific wear rates of the Ti64 substrate and coating indicate that the tribological properties of the Ti64 coating used in this study are comparable to those of the commercial Ti64 substrate.

In Fig. 9, the sliding of the steel balls on the surfaces and cross section of the Ti64 coating gives rise to a stable friction during the entire sliding as a result of the stable wear of rubbing surfaces (Ref 19, 25-27).

Figure 10(a), (b), and (c) show the wear topographies and morphologies of the Ti64 coating on its different layers. Abrasive grooves are found on all the wear tracks of the Ti64 coating as a result of their significant abrasive wear caused by the repeated sliding of the steel ball (Ref 18, 19, 25-27). Although the sliding of the steel ball on the cross section of the Ti64 coating generates an apparent wear track via abrasive wear (Fig. 10d), the wear track on

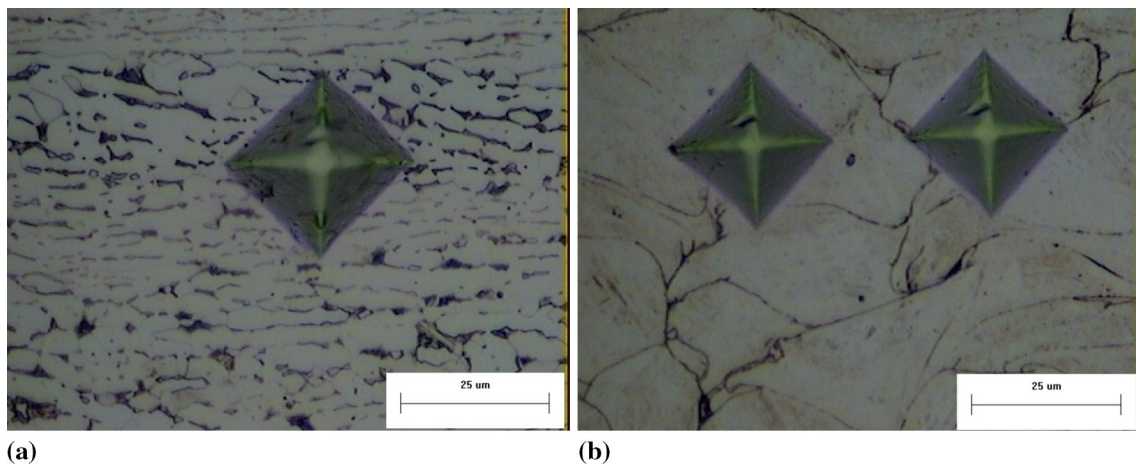


Fig. 8 OM images showing indents on the cross-sectional microstructures of (a) Ti64 substrate and (b) Ti64 coating, made using a normal load of 200 g

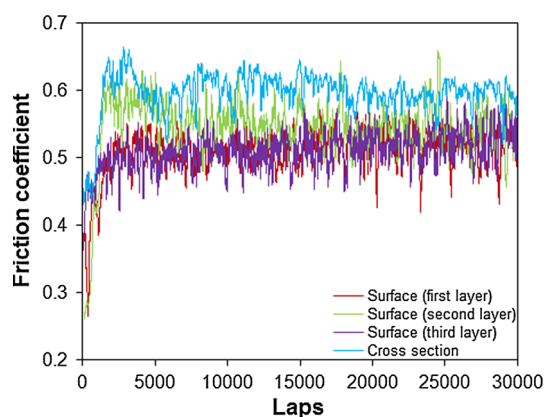


Fig. 9 Friction coefficients of Ti64 coating, tested against a 100Cr6 steel ball of 6 mm in diameter in a circular path of 1 mm in radius for 30,000 laps at a sliding speed of 3 cm/s under a normal load of 1 N, as a function of the number of laps

the cross section (Fig. 10d) is apparently smaller than those on the surfaces (Fig. 10a, b, and c), which confirms that the cross section of the Ti64 coating is more resistant to abrasive wear than its surface probably due to the higher cross-sectional hardness of the coating. The Ti64 coating has rougher wear morphologies and larger amount of wear debris on its surface wear tracks (Fig. 10a, b, and c) compared to its cross-sectional wear track (Fig. 10d).

The sliding of the steel ball on the cross section of the Ti64 coating generates a friction coefficient of 0.60 ± 0.01 that is higher than those resulted from the sliding of the steel ball on the surfaces of the different layers of the same coating. It was reported that adhesion between two smooth surfaces in contact could generate high friction via an effective interfacial shear strength between them (Ref 19, 25-33). Wear of rubbing surfaces can roughen them, which in turn reduces the real contact area to lessen the interfacial shear strength and consequently lowers the friction (Ref 19, 25-33). At the same time, the wear debris released between the rubbing surfaces prevent a direct contact between them. Debris particles freely roll or slide under a lateral force, which leads to a decrease in friction (Ref 19, 25-33). Therefore, the higher cross-sectional wear resistance of the Ti64 coating than its surface wear resistance results in the higher friction via less surface roughening and smaller amount of wear debris (Fig. 10), which is confirmed by the lower specific wear rate ($81.9 \pm 16.9 \times 10^{-14} \text{ m}^3/(\text{Nm})$) of the cross section of the Ti64 coating compared to those of its surfaces at different layers.

Figure 11(a) shows the wear morphology of the first layer of the Ti64 coating on which abrasive grooves are found. It confirms that wear of the Ti64 coating tested against the steel ball is attributed to abrasive wear (Ref 12-14, 19, 25-27). In addition, a removal of materials from

deep regions as platelets is found on the wear track of the Ti64 coating (Ref 19, 25, 34, 35). The reason is that the repeated sliding of the steel ball initiates minute cracks in the subsurface and allows them to propagate parallel to free surface for some extent so that it eventually leads to a removal of materials from deep regions as platelets via surface fatigue (Ref 19, 25, 34, 35). It is clear that fatigue wear also contributes to wear of the Ti64 coating in the dry conditions. Comparison of Fig. 11(a) and (b) shows that the cross-sectional wear track of the Ti64 coating has fewer abrasive grooves and does not exhibit material removal from deep regions, in comparison with the surface wear track, which indicates that the cross section of the Ti64 coating is more resistant to abrasive and fatigue wear.

Figure 12(a) shows the EDX spectrum measured on the untested area of the Ti64 coating on which Ti, Al, and V peaks are found without an apparent observation of O peak. The Ti, Al, and V peaks are mainly attributed to the Ti matrix, while the lack of O peak indicates that oxidation of sprayed Ti64 particles has not occurred during cold spraying (Ref 19, 25-27). However, the EDX spectra measured on the wear tracks of the Ti64 coating (Fig. 12b, c, and d) exhibit an additional O peak because the rubbing of the steel ball on the coating surface induces an oxidation process via frictional heating (Ref 19, 25-27). Similar EDX spectra are found for the surface (Fig. 12b, c, and d) and cross-sectional (Fig. 12e) wear tracks of the Ti64 coating as a result of the similar wear mechanisms occurred during rubbing contact with the steel ball.

Figure 12(f) shows the wear morphology of the steel ball rubbed on the surface of the first layer of the Ti64 coating on which apparent abrasive lines are found as a result of abrasive wear.

Corrosion of Ti64 Coating

Figure 13(a) shows the OCPs of the Ti64 substrate and coating immersed in the 0.6 M NaCl solution as a function of time. The OCP of the Ti64 coating shifts to more negative values at the beginning due to the dissolution of an oxide film that was spontaneously formed on the coating surface due to exposure to the atmosphere (Ref 36). Then, the OCP of the coating slowly shifts to more positive values as a result of the formation of a passive film composed mainly of metal oxides such as TiO_2 , Al_2O_3 , and V-oxides (Ref 36-38). However, the Ti64 substrate shows a continuous increase in its OCP during the 24 h long immersion probably due to the continuous formation of a passive film on its surface (Ref 36-38). It is clear that the Ti64 coating exhibits higher OCP than the Ti64 substrate throughout the immersion test, which means that the Ti64 coating is electrochemically nobler and has an equilibrium condition between its dissolution and protection with the

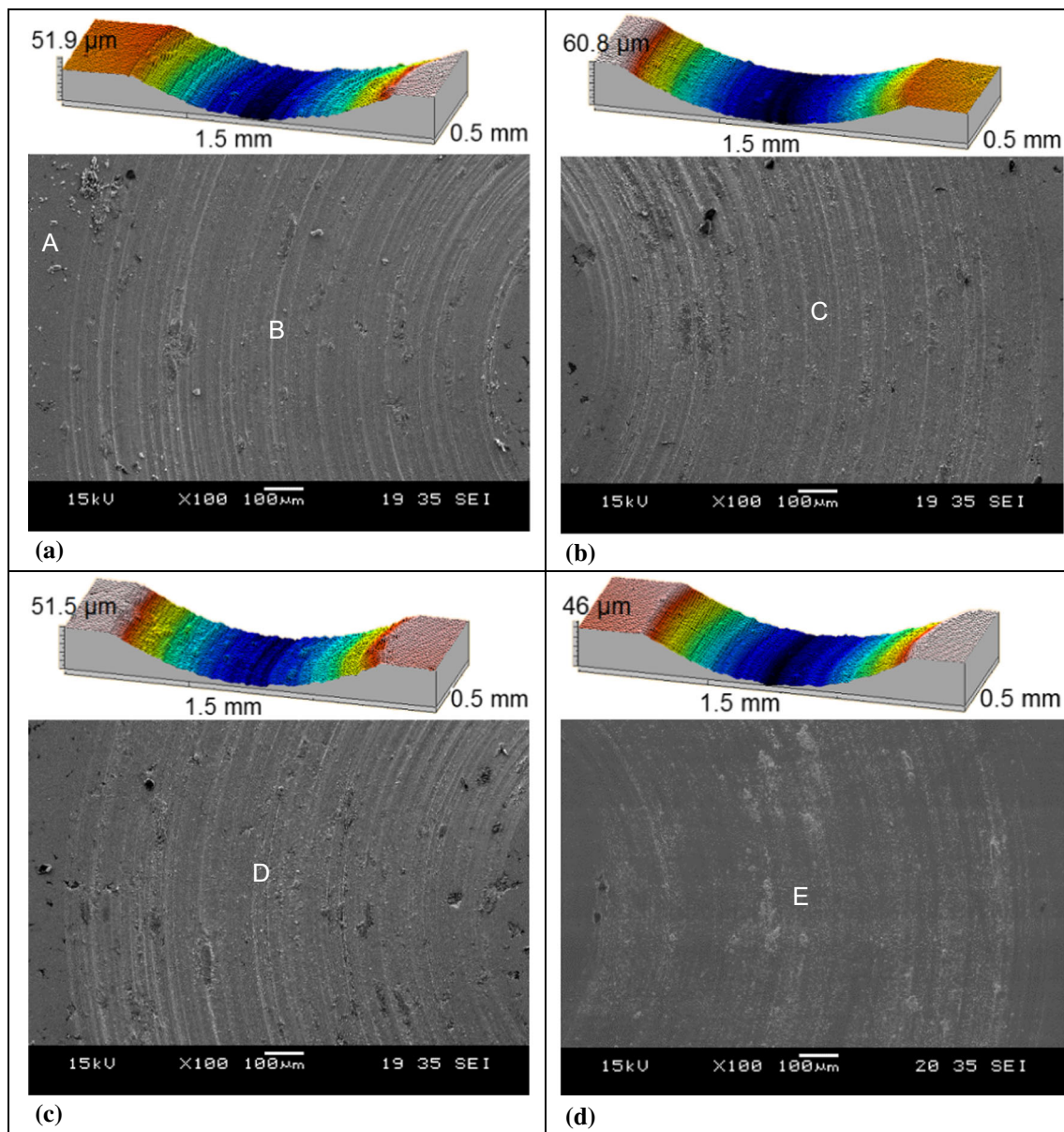


Fig. 10 Wear topographies (above) and morphologies (below) of Ti64 coating tested under the same condition as described in Fig. 9: (a) surface of the first layer, (b) surface of the second layer, (c) surface of the third layer, and (d) cross section

formation of an oxide film at more positive potentials (Ref 36-38).

Figure 13(b) illustrates the potentiodynamic polarization curves of the Ti64 substrate and coating measured in the 0.6 M NaCl solution for different immersion periods. In Table 1, the E_{corr} and i_{corr} of the Ti64 substrate immersed in the NaCl solution for 4 h are about -252 mV versus Ag/AgCl and 8.3×10^{-8} A/cm², respectively. Increasing the immersion time to 24 h apparently shifts the E_{corr} to -135 mV versus Ag/AgCl and the i_{corr} to 1.2×10^{-8} A/cm², respectively, as presented in Fig. 13(b) and Table 1. It indicates that longer immersion in the NaCl solution gives rise to slower anodic dissolution of the Ti64 substrate via

the continuous formation of a passive film on its surface (Ref 36-38). The E_{corr} and i_{corr} of the Ti64 coating after 4 h are about -20 mV versus Ag/AgCl and 34.3×10^{-6} A/cm² and shift to -29.6 mV versus Ag/AgCl and 48.2×10^{-5} A/cm² after the 24 h long immersion, respectively (Fig. 13b and Table 1). It can be seen that there is an increase in the corrosion rate of the Ti64 coating during prolonged immersion in the NaCl solution. The polarization results show that the E_{corr} of the Ti64 coating is nobler than that of the Ti64 substrate during the entire immersion, which implies that the Ti64 coating is electrochemically more stable at more positive potentials (Ref 13, 20-22). However, the i_{corr} of the Ti64 coating is

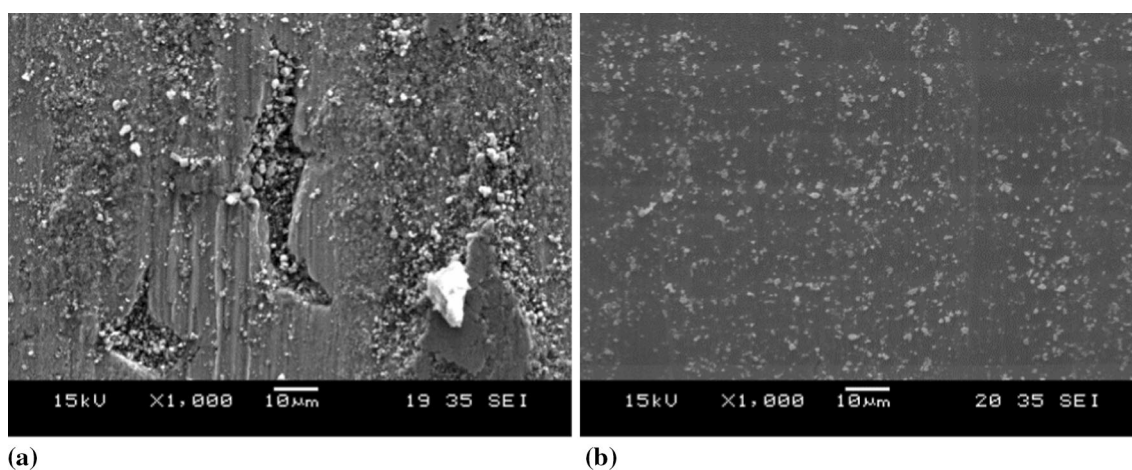


Fig. 11 Wear morphologies of Ti64 coating, tested under the same condition as described in Fig. 9, observed at a high magnification: (a) surface of the first layer, and (b) cross section

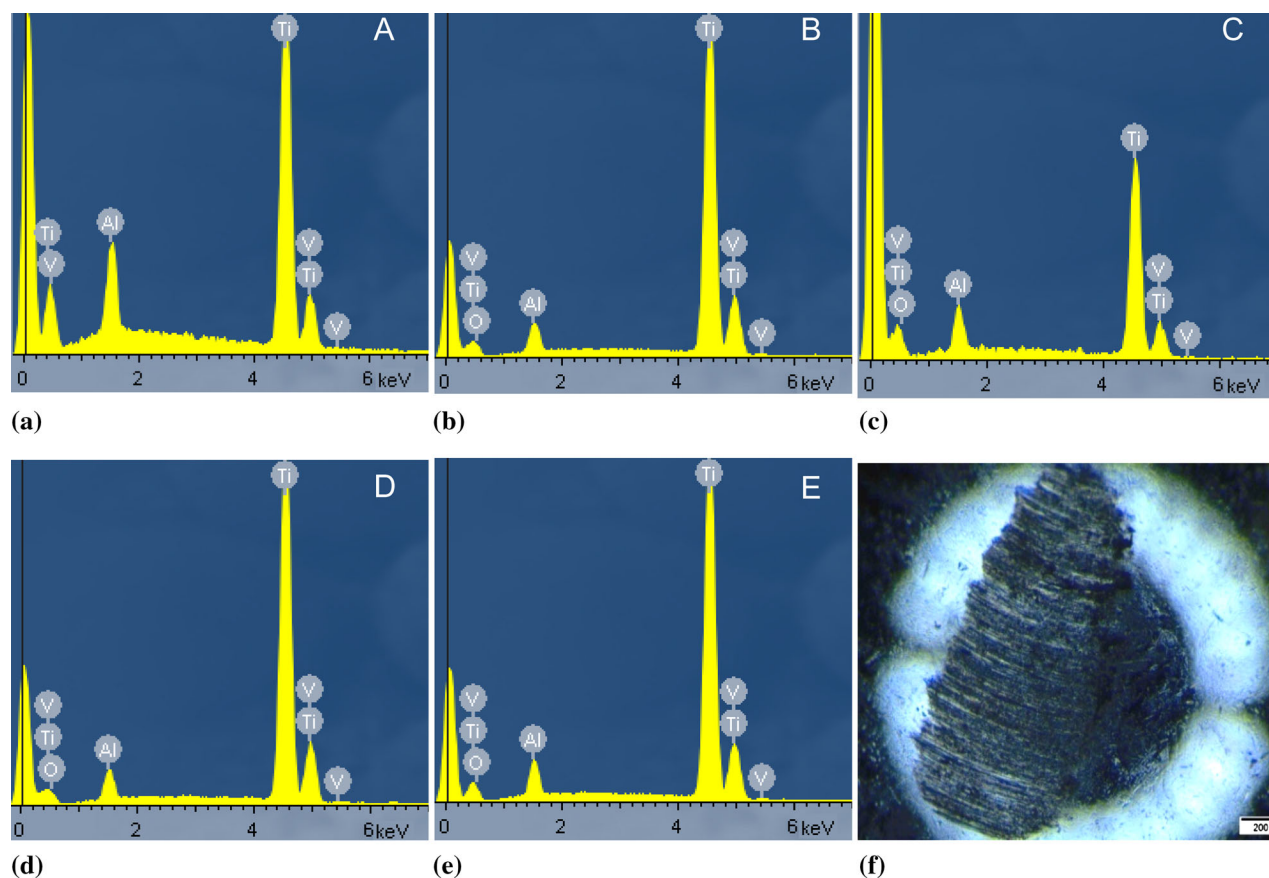


Fig. 12 EDX spectra of Ti64 coating measured on its (a) untested and (b, c, d, and e) tested areas at locations (a) A in Fig. 10(a), (b) B in Fig. 10(a), (c) C in Fig. 10(b), (d) D in Fig. 10(c), and (e) E in Fig. 10(d). (f) OM image showing the wear morphology of the steel ball slide on the surface of the first layer of the Ti64 coating under the same condition as described in Fig. 9

apparently higher than that of the Ti64 substrate, indicating that the Ti64 coating releases more ions in the NaCl solution than the Ti64 substrate. The possible reason is that the Ti64 coating with a significant number of micropores

and particle interfaces has a much larger exposed area to the NaCl solution to release much more metal ions compared to the Ti64 substrate although the Ti64 coating is electrochemically nobler (Ref 13, 20–22). In addition, the

anodic dissolution of the coating/substrate interface in the NaCl solution can contribute to the higher i_{corr} of the Ti64 coating (Ref 13, 20-22).

Figure 14(a) and (b) show the Nyquist plots of the Ti64 substrate and coating, respectively, immersed in the 0.6 M NaCl solution as a function of time. In Fig. 14(a), the Nyquist plots of the Ti64 substrate contain incomplete semicircles and the diameter of the semicircles becomes larger with longer immersion as a result of the enhanced surface passivation of the Ti64 substrate (Ref 36-38). As shown in Fig. 14(b), incomplete and depressed semicircles are found in the Nyquist plots of the Ti64 coating. The diameter of the semicircles produced by the Ti64 coating in the Nyquist plots slightly decreases with increasing immersion time due to the increased corrosion rate of the

Ti64 coating in the NaCl solution (Ref 20-22, 39, 40). Comparison of Fig. 14(a) and (b) therefore confirms that the Ti64 coating has higher dissolution rate in the NaCl solution than does the Ti64 substrate, probably due to the much larger exposed area of the Ti64 coating to the NaCl solution, as noted previously.

The Bode plots of the Ti64 substrate and coating with respect to time are reported in Fig. 14(c) and (d), respectively. Normally, an ideal capacitive behavior would result in a slope of -1 and a phase angle of -90° (Ref 39-42). In Fig. 14(c), the phase angles of the Ti64 substrate in the low-frequency range become closer to -90° with longer immersion, which is indicative of the improved quality of the passive oxide film on its surface. In Fig. 14(d), the phase angles of the Ti64 coating in the low-frequency range apparently deviate from -90° probably due to the porous structure of the Ti64 coating since the phase angles in the low-frequency range are related to the bulk properties of the coating. As shown by comparison of Fig. 14(c) and (d), the Ti64-coated sample has apparently smaller $|Z|$ values at 0.01 Hz for all the immersion times than the uncoated sample because micropores and particle interfaces in the coating induce higher dissolution in the NaCl solution (Ref 39-42).

Figure 15(a) and (b) show the proposed equivalent circuits for the Ti64 substrate and coating immersed in the 0.6 M NaCl solution, respectively. In the equivalent circuit of the Ti64 substrate (Fig. 15a), R_1 , R_2 , and Y_2 represent the solution resistance, and the charge transfer resistance and double-layer capacitance at the solution/substrate interface, respectively. In the equivalent circuit of the Ti64 coating (Fig. 15b), R_1 , R_2 , Y_2 , R_3 , and Y_3 represent the solution resistance, the pore resistance and capacitance of the coating, and the charge transfer resistance and double-layer capacitance at the solution/substrate interface below the bases of pores, respectively. In this study, the capacitance is replaced with a constant phase element (Y).

The EIS results determined from the EIS spectra presented in Fig. 14 using the equivalent circuits proposed in Fig. 15 are reported in Table 2. It is found that the increased immersion time from 4 to 24 h increases the R_2 value of the Ti64 substrate from 1×10^6 to

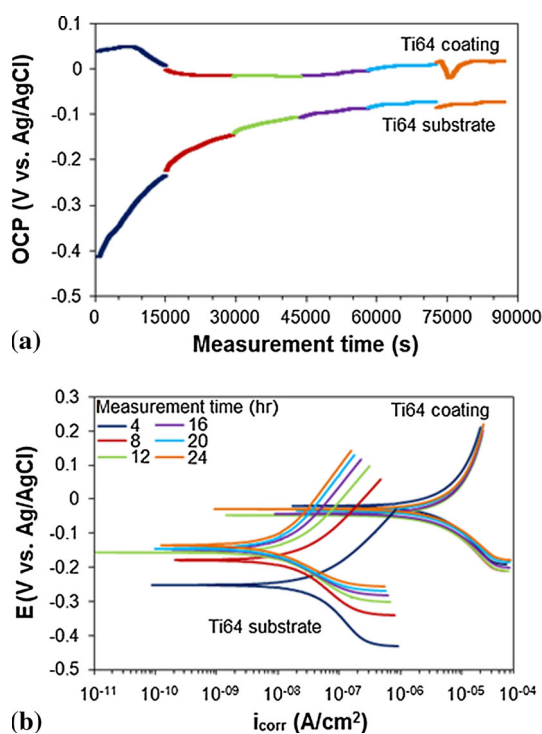


Fig. 13 (a) Open-circuit potentials (OCPs) and (b) potentiodynamic polarization curves of Ti64 substrate and Ti64 coating immersed in 0.6 M NaCl solution for different immersion periods

Table 1 Corrosion results determined from potentiodynamic polarization curves of Ti64 substrate and Ti64 coating presented in Fig. 13b

Measurement time, h	Ti64 substrate		Ti64 coating	
	E_{corr} , mV	I_{corr} , A/cm ²	E_{corr} , mV	I_{corr} , A/cm ²
4	-252	8.3×10^{-8}	-20	34.3×10^{-6}
8	-179	3.5×10^{-8}	-44.2	35.3×10^{-6}
12	-157	2×10^{-8}	-48	66.9×10^{-5}
16	-149	1.4×10^{-8}	-42.5	97.8×10^{-5}
20	-144	1.3×10^{-8}	-33.7	17.7×10^{-6}
24	-135	1.2×10^{-8}	-29.6	48.2×10^{-5}

Fig. 14 (a and b) Nyquist and (c and d) Bode plots of (a and c) Ti64 substrate and (b and d) Ti64 coating immersed in 0.6 M NaCl solution for different immersion periods

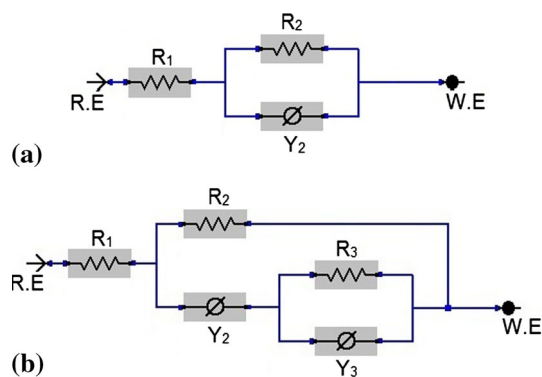
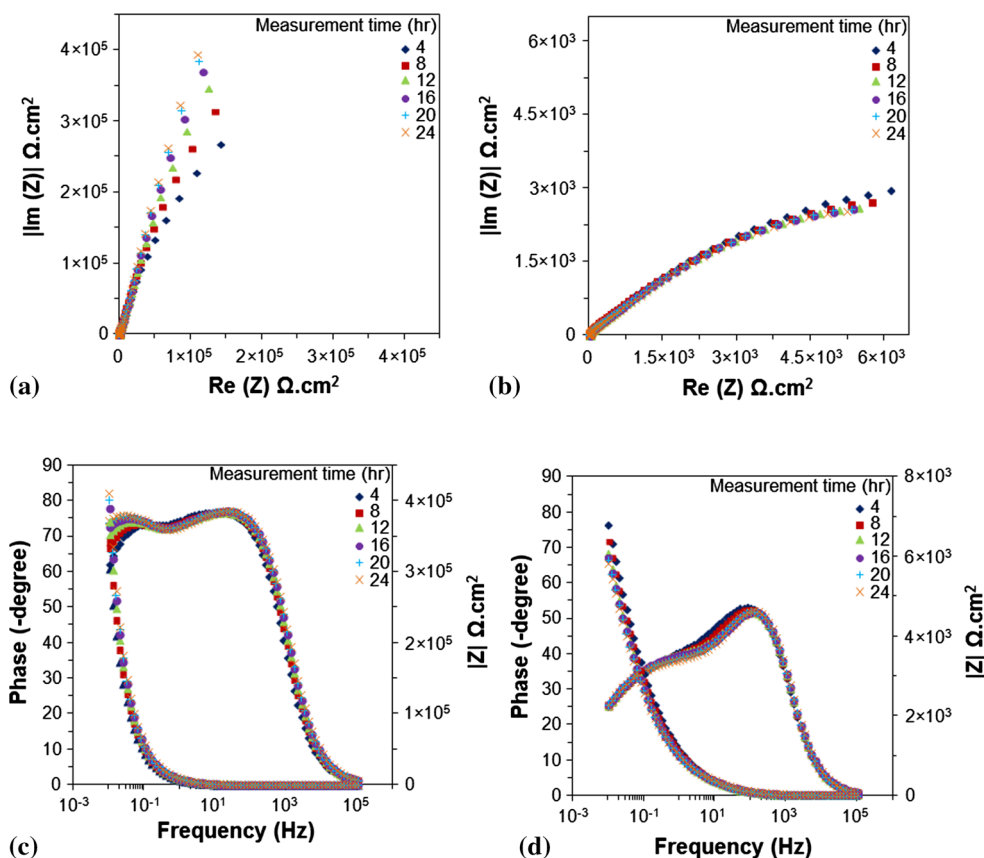


Fig. 15 Equivalent circuits of (a) Ti64 substrate and (b) Ti64 coating immersed in 0.6 M NaCl solution

$7.1 \times 10^6 \Omega \text{ cm}^2$ as a result of its enhanced surface passivation (Ref 36-38). The R_2 value of the Ti64 coating decreases from 9.1×10^3 to $8 \times 10^3 \Omega \text{ cm}^2$ with increased immersion time from 4 to 24 h, indicating that the pore resistance of the Ti64 coating decreases during prolonged immersion in the NaCl solution because the increased permeation of the NaCl solution into the coating increases the ionic conduction of the coating (Ref 39-42). The Y_2 value of the Ti64 coating increases from 32.6×10^{-5} to $42.6 \times 10^{-5} \text{ S}^n/\Omega \text{ cm}^2$ with increased immersion time from 4 to 24 h (Table 2). It indicates that

the increase in the coating capacitance is attributed to an increase in the water uptake (Ref 43). The R_3 values of the Ti64 coating at 4 and 24 h are 6.1×10^2 and $3.9 \times 10^2 \Omega \text{ cm}^2$, respectively, which indicates that the charge transfer resistance at the solution/substrate interface is lower for the longer immersion (Ref 39-42). Underneath the Ti64 coating, the Ti64 substrate does not exhibit the formation of a passive oxide film on its surface to retard its surface corrosion. The possible reason is that the narrow interfacial gaps between the coating and the substrate below the bases of pores serve as confined spaces so that the concentrations of H^+ and Cl^- inside the confined spaces become increasing high over the prolonged immersion to result in a breakage of the passive oxide film and a subsequent increase in the corrosion rate of the Ti64 substrate with increased immersion time via crevice corrosion (Ref 44, 45). In addition, a galvanic corrosion between the substrate and the coating can reduce the charge transfer resistance at the solution/substrate interface during the prolonged immersion (Ref 44, 46). The corrosion results clearly show that the corrosion behavior of the Ti64-coated sample is significantly different from that of the uncoated sample.

Figure 16(a) and (b) show the surface morphologies of the Ti64 substrate and coating after immersion in the 0.6 M NaCl solution for 24 h, respectively. Although both the

Table 2 EIS results determined from EIS spectra presented in Fig. 14 using the equivalent circuits proposed in Fig. 15

Measurement time, h	$R_1, \Omega \text{ cm}^2$	$R_2, \Omega \text{ cm}^2$	$Y_2, \text{S}^n/\Omega \text{ cm}^2$	N_2	$R_3, \Omega \text{ cm}^2$	$Y_3, \text{S}^n/\Omega \text{ cm}^2$	N_3
Ti64 substrate							
4	18.2	1×10^6	32.2×10^{-6}	0.859
8	18	1.6×10^6	29.2×10^{-6}	0.853
12	18	2.6×10^6	27.6×10^{-6}	0.851
16	18	3.8×10^6	26.4×10^{-6}	0.85
20	18	5.3×10^6	25.6×10^{-6}	0.849
24	17.8	7.1×10^6	25.1×10^{-6}	0.848
Ti64 coating							
4	16.5	9.1×10^3	32.6×10^{-5}	0.668	6.1×10^2	15.8×10^{-5}	0.755
8	16.4	8.5×10^3	38.6×10^{-5}	0.658	4.8×10^2	14.3×10^{-5}	0.77
12	16.3	8.2×10^3	40.3×10^{-5}	0.648	3.9×10^2	13.2×10^{-5}	0.782
16	16.3	8.1×10^3	41×10^{-5}	0.644	3.7×10^2	12.3×10^{-5}	0.789
20	16.3	8.1×10^3	41.6×10^{-5}	0.644	3.9×10^2	11.9×10^{-5}	0.788
24	16.3	8×10^3	42.6×10^{-5}	0.643	3.9×10^2	11.5×10^{-5}	0.788

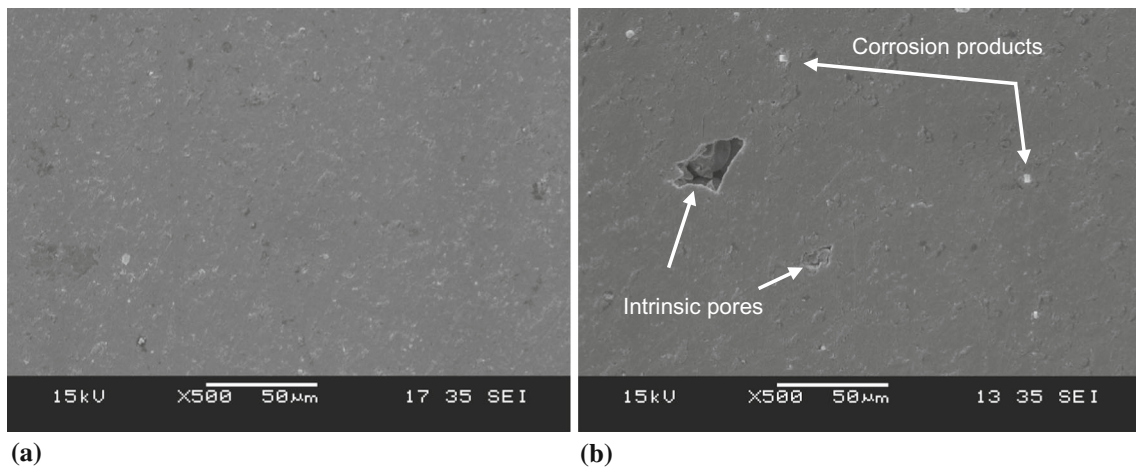


Fig. 16 Surface morphologies of (a) Ti64 substrate and (b) Ti64 coating after immersion in 0.6 M NaCl solution for 24 h

Ti64 substrate and the coating do not show severe corrosion during the 24 h long immersion in the NaCl solution, the Ti64 coating seems to have more corrosion products on the surface than does the Ti64 substrate because the higher dissolution rate of the Ti64 coating in the NaCl solution allows more electrochemical reactions between its surface and the corrosion medium to form the corrosion products (Ref 13).

Conclusions

In this study, a 9-mm-thick Ti64 coating was deposited on a commercial Ti64 substrate via a high-pressure cold spray process. The Ti64 coating showed similar surface

microstructures at different layers although a significant number of pores were found on all the surfaces. An apparent deformation of sprayed Ti64 particles caused by the cold spraying was found in the cross-sectional microstructure of the Ti64 coating. The hardness of the Ti64 coating was higher than that of the Ti64 substrate as a result of the cold-worked microstructure of the coating. The tribological results showed that the specific wear rates of the Ti64 coating, measured on different layers, were not very much different from each other due to the similar microstructures of all the layers. The corrosion results showed that the Ti64 coating was electrochemically nobler in the 0.6 M NaCl solution than the Ti64 substrate although the Ti64 coating had higher corrosion current density than the Ti64 substrate due to the much larger exposed area of

the coating to the NaCl solution. The electrochemical impedance spectroscopy (EIS) results confirmed that the Ti64-coated sample had lower charge transfer resistance than the uncoated sample. It could be concluded that the cold spray process could be applied to produce the 9-mm-thick Ti64 coating with comparable mechanical and tribological properties to those of the commercial Ti64 substrate although the thick Ti64 coating could not effectively prevent its underlying Ti64 substrate from corrosion.

References

1. C. Leyens and M. Peters, *Titanium and titanium alloys: fundamentals and applications*, Wiley, Weinheim, 2006
2. R. Boyer, E.W. Collings, and G. Welsch, *Materials properties: titanium alloys*, ASM International, Russell Township, 1994
3. F.M. Kustas and M.S. Misra, Friction and Wear of Titanium Alloys, in *Lubrication, and wear technology*, ASM Handbook, vol 18, P.J. Blau, Ed., ASM International, 1992, p. 778-784
4. R.W. Schutz, Corrosion of Titanium and Titanium Alloys, in *Corrosion: Materials*, ASM Handbook, vol 13B, S.D. Cramer and B.S. Covino, Jr., Ed., ASM International, 2005, p. 252-299
5. R. Walker and B. Barnes, High-Velocity Oxygen Fuel Spray Coatings for Reclamation, *Mater. Des.*, 1994, **15**(6), p 323-329
6. M. Froning, P. Ruggiero, J. Tsiao, J. Marnix, C. Alford, and G. Shubert, Transition of a World Class HVOF Thermal Spray Capability into a US Engine Overhaul Facility, in *Thermal spray solutions, Advances in Technology and Application: Proceedings of the International Thermal Spray Conference 2004* (Osaka, JP), DVS, Düsseldorf, Germany
7. A. Kumar, J. Boy, R. Zatorski, and L.D. Stephenson, Thermal Spray and Weld Repair Alloys for the Repair of Cavitation Damage in Turbines and Pumps: A Technical Note, *J. Therm. Spray Technol.*, 2005, **14**(2), p 177-182
8. J.C. Tan, L. Looney, and M.S.J. Hashmi, Component Repair Using HVOF Thermal Spraying, *J. Mater. Process. Technol.*, 1999, **92-93**, p 203-208
9. N. Bala, H. Singh, J. Karthikeyan, and S. Prakash, Cold Spray Coating Process for Corrosion Protection: A Review, *Surf. Eng.*, 2014, **30**(6), p 414-421
10. H. Singh, T.S. Sidhu, and S.B.S. Kalsi, Cold Spray Technology: Future of Coating Deposition Processes, *Frattura ed Integrità Strutturale*, 2012, **22**, p 69-84
11. H. Assadi, T. Schmidt, H. Richter, J.O. Kliemann, K. Binder, F. Gartner, T. Klassen, and H. Kreye, On Parameter Selection in Cold Spraying, *J. Therm. Spray Technol.*, 2011, **20**(6), p 1161-1176
12. N.W. Khun, A.W.Y. Tan, and E. Liu, Mechanical and Tribological Properties of Cold Sprayed Ti Coatings on Ti-6Al-4V Substrates, *J. Therm. Spray Technol.*, 2016, **25**(4), p 715-724
13. N.W. Khun, A.W.Y. Tan, and E. Liu, Effect of Working Pressure on Wear and Corrosion Resistance of Cold Sprayed Ti-6Al-4V Coatings, *Surf. Coat. Technol.*, 2016, **302**, p 1-12
14. N.W. Khun, A.W.Y. Tan, W. Sun, and E. Liu, Effect of Heat Treatment Temperature on Microstructure, and Mechanical and Tribological Properties of Cold Sprayed Ti-6Al-4V Coatings, *Tribol. Trans.*, 2016, doi:[10.1080/10402004.2016.1244584](https://doi.org/10.1080/10402004.2016.1244584)
15. S.V. Klinkov, V.F. Kosarev, and M. Rein, Cold Spray Deposition: Significance of Particle Impact Phenomena, *Aerosp. Sci. Technol.*, 2005, **9**, p 582-591
16. K.G. Budinski, Tribological Properties of Titanium Alloys, *Wear*, 1991, **151**(2), p 203-217
17. Q. Niu, X. Zheng, M. Chen, and W. Ming, Study on the Tribological Properties of Titanium Alloys Sliding Against WC-CO During the Dry Friction, *Ind. Lubr. Tribol.*, 2014, **66**(2), p 202-208
18. S.B. Pitchuka, B. Boesl, C. Zhang, D. Lahiri, A. Nieto, G. Sundararajan, and A. Agarwal, Dry Sliding Wear Behavior of Cold Sprayed Aluminum Amorphous/Nanocrystalline Alloy Coatings, *Surf. Coat. Technol.*, 2014, **238**, p 118-125
19. N.W. Khun, R.T. Li, K. Loke, and K.A. Khor, Effects of Al-Cr-Fe Quasicrystal Content on Tribological Properties of Cold Sprayed Titanium Composite Coatings, *Tribol. Trans.*, 2015, **58**(4), p 616-624
20. K. Ishikawa, T. Suzuki, Y. Kitamura, and S. Tobe, Corrosion Resistance of Thermal Sprayed Titanium Coatings in Chloride Solution, *J. Therm. Spray Technol.*, 1999, **8**(2), p 273-278
21. T. Hussian, D.G. McCartney, P.H. Shipway, and T. Marrocco, Corrosion Behaviour of Cold Sprayed Titanium Coatings and Free Standing Deposits, *J. Therm. Spray Technol.*, 2011, **20**(1-2), p 260-274
22. H.R. Wang, W.Y. Li, J. Wang, and Q. Wang, Corrosion Behaviour of Cold Sprayed Titanium Protective Coating on 1Cr13 Substrate in Seawater, *Surf. Coat. Technol.*, 2007, **201**(9-11), p 5203-5206
23. H. Assadi, F. Gartner, T. Stoltenhoff, and H. Kreye, Bonding mechanism in cold gas spraying, *Acta Mater.*, 2003, **51**, p 4379-4394
24. R. Huang, M. Sone, W. Ma, and H. Fukunuma, The Effect of Heat Treatment on the Mechanical Properties of Cold Sprayed Coatings, *Surf. Coat. Technol.*, 2015, **261**, p 278-288
25. N.W. Khun, R.T. Li, and K.A. Khor, Mechanical and Tribological Properties of Spark Plasma Sintered Titanium Composites Filled with Different Al-Cr-Fe Quasicrystal Content, *Tribol. Trans.*, 2015, **58**(5), p 859-866
26. N.W. Khun, G.S. Frankel, and M. Sumption, Effects of Normal Load, Sliding Speed and Surface Roughness on Tribological Properties of Niobium Under Dry and Wet Conditions, *Tribol. Trans.*, 2014, **57**(5), p 944-954
27. N.W. Khun, E. Liu, A.W.Y. Tan, D. Senthilkumar, B. Albert, and D.M. Lal, Effects of Deep Cryogenic Treatment on Mechanical and Tribological Properties of AISI, D3 Tool Steel, *Friction*, 2015, **3**(3), p 234-242
28. J.H.W. Siu and L.K.Y. Li, An Investigation of the Effect of Surface Roughness and Coating Thickness on the Friction and Wear Behaviour of a Commercial MoS₂-Metal Coating on AISI, 400C Steel, *Wear*, 2000, **237**(2), p 283-287
29. P.J. Blau, *Friction science and technology*, Marcel Dekker, New York, 1996
30. K. Kato, Wear in Relation to Friction: Review, *Wear*, 2005, **241**, p 151-157
31. C.M. Mate, *Tribology on the Small Scale: a Bottom Up Approach to Friction, Lubrication and Wear*, 1st ed., Oxford University Press, Oxford, 2008
32. H. Ronkainen, A. Laukkanen, and K. Holmberg, Friction in a Coated Surface Deformed by a Sliding Sphere, *Wear*, 2007, **263**(7-12), p 1315-1323
33. B. Bhushan, *Tribology and Mechanics of Magnetic Storage Device*, 2nd ed., Springer, New York, 1996
34. S. Stewart and R. Ahmed, Rolling Contact Fatigue of Surface Coatings: Review, *Wear*, 2002, **253**, p 1132-1144
35. S.H. Teoh, Fatigue of Biomaterials: a Review, *Int. J. Fatigue*, 2000, **22**, p 825-837
36. E.S.M. Sherif, A.A. Almajid, K.A. Khalil, H. Junaedi, and F.H. Latief, Electrochemical Studies on the Corrosion Behaviour of

- API, X65 Pipeline Steel in Chloride Solutions, *Int. J. Electrochem. Sci.*, 2013, **8**, p 9360-9370
37. R.M.A. Shahba, W.A. Ghannem, A.E.S. El-Shenawy, A.S.I. Ahemd, and S.M. Tantawy, Corrosion and Inhibition of Ti-6Al-4V Alloy in NaCl Solution, *Int. J. Electrochem. Sci.*, 2011, **6**, p 5499-5509
38. H.J. Song, M.K. Kim, G.C. Jung, M.S. Vang, and Y.J. Park, The Effect of Spark Anodizing Treatment of Pure Titanium Metals and Titanium Alloys on Corrosion Characteristics, *Surf. Coat. Technol.*, 2007, **201**(21), p 8738-8745
39. N.W. Khun and G.S. Frankel, Effect of Hexafluorozirconic Acid Pretreatment on Cathodic Delamination of Epoxy Coatings from Steel Substrates, *Corrosion*, 2015, **71**(3), p 277-284
40. N.W. Khun and G.S. Frankel, Composition and Corrosion Protection of Hexafluorozirconic Acid Treatment on Steel, *Mater. Corros.*, 2015, **66**(11), p 1215-1222
41. A. Zeng, E. Liu, I.F. Annergren, S.N. Tan, S. Zhang, P. Hing, and J. Gao, EIS capacitance Diagnosis of Nanoporosity Effect on the Corrosion Protection of DLC Films, *Diam. Relat. Mater.*, 2002, **11**, p 160-168
42. S.M. Bhola and B. Mishra, Effect of pH on the Electrochemical Properties of Oxides Formed over α -Ti-15Mo and Mixed Ti-6Al-4V Alloys, *Int. J. Electrochem. Sci.*, 2013, **8**, p 7075-7087
43. C. Moreno, S. Hernández, J.J. Santana, J. González-Guzmán, R.M. Souto, and S. González, Characterization of Water Uptake by Organic Coatings Used for the Corrosion Protection of Steel as Determined from Capacitance Measurements, *Int. J. Electrochem. Sci.*, 2012, **7**, p 8444-8457
44. N.W. Khun, E. Liu, and X.T. Zeng, Corrosion Behaviour of Nitrogen Doped Diamond-Like Carbon Thin Films in NaCl Solution, *Corros. Sci.*, 2009, **51**(9), p 2158-2164
45. E.M. Fayyad, M.A. Almaadeed, A. Jones, and A.M. Abdullah, Evaluation Techniques for the Corrosion Resistance of Self-Healing Coatings, *Int. J. Electrochem. Sci.*, 2014, **9**, p 4989-5011
46. S. Kuroda, J. Kawakita, T. Fukushima, and S. Tobe, Importance of the Adhesion of HVOF Sprayed Coatings for Aqueous Corrosion Resistance, *Mater. Trans.*, 2003, **44**(3), p 381-388